nature geoscience

SUPPLEMENTARY INFORMATION

DOI: 10.1038/NGEO2139

# Carbon sequestration during the Palaeocene–Eocene Thermal Maximum by an efficient biological pump

Zhongwu Ma[1#], Ellen Gray[1], Ellen Thomas[2], Brandon Murphy[1], James Zachos[1], Adina Paytan[1*]

[1]Earth and Planetary Science, University of California Santa Cruz, 1156 High Street, Santa Cruz, CA, 95064

[2]Department of Geology & Geophysics, Yale University, P.O. Box 208109, New Haven, Connecticut 06520-8109, USA

*Corresponding author: apaytan@ucsc.edu

#Current address: Laboratory for Earth Surface Processes, Department of Geography,

Peking University, Beijing, 100871, China

## Supplemental Materials

### Barite Formation and Preservation

Barite formation in the ocean is closely related to export production[1-5]. Accordingly, barite accumulation rates (BAR) have been used as a proxy for export production at multiple sites and time scales[6-15]. The ocean is undersaturated with respect to barite however, barite crystals form in the water column abiotically within microenvironments in association with decaying organic matter and other biological debris and in proportion to the organic matter content [1, 3, 16-18]. This is supported by field observations[19], laboratory experiments[20] and the depth distribution of dissolved Ba and particulate barite in the water column[1, 4, 21, 22]. Consequently, higher accumulation of barite indicates that more organic carbon was transported to the deep ocean and sediment (see review by Paytan and Griffith[5]).

Once the barite is buried, regeneration of various Ba carrying phases within the upper few centimeters of the sediment results in barite saturation in pore fluids thus the remaining barite is preserved in sediments that do not undergo sulfate reduction[5, 23]. In sediments where sulfate reduction rates are high barite preservation is compromised and this proxy cannot be used for reconstructing export production[24-26].

Due to extensive sulfate reduction and barite remobilization is shallow coastal settings with high organic C content, and the potential formation of barite in pore-fluids [24, 25, 27, 28], near shore coastal settings were not included in this work. In this study, we reconstruct BAR across the PETM in the world's open ocean basins where pore water sulfate is not

substantially depleted (based on DSDP/ODP data). To confirm the biogenic (not diagenetic) origin of the barite at our site each sample was also screened visually and chemically for origin and following[26, 29] (see below).

## Methods

*Study sites*

More than 210 samples selected from 12 DSDP and ODP sites at location in the Pacific, Atlantic, Indian and Southern Ocean were analyzed for weight percent barite which was then converted to barite accumulation rates and used to reconstruct the world-wide export productivity during PETM (Figure 1, Tables S1, S2). Each of these cores was sampled over the PETM at a depth resolution of between 30 cm to 2 m which resulted in different temporal resolution, depending on the sedimentation rate at each site. Each sample consists of 10-20 grams of dry sediment typically from 1 to 5 cm sections, with a few samples combining sediment from up to 50 cm sections depending on sample availability. Each sample thus typically represents several thousands to more than 30,000 years of accumulation (depending on sedimentation rates).

*Barite separation*

Barite was separated from the sediment using a sequential leaching extraction protocol which dissolves the other constituents of the sediment, leaving behind barite and a few other minor refractory minerals[13]. For samples containing less than 95% barite in the

residue or if other contaminants were detected further purification was done by dissolution and re-precipitation of barite using the procedure of Breit et al.[30]. The barite recovery yield for this procedure is typically > 95%[13]. In order to determine the barite fraction in the residue we used a JOEL 5600 Scanning Electron Microscope with an EDAX Spectrum Analysis program. The percentage of barite present in the residue was determined from a pixilation count of the percentage of the screen it occupies. Comparison between this method and the direct determination of barite content by dissolution and analysis of Ba and/or sulfate yields comparable results. The weight percent barite (wt% Barite) in each sample was calculated based on the weights of the dry sediment used, the weight of the final residue and the barite fraction in the residual sample.

Because barite is a minor component of marine sediments barite content may be controlled primarily by changes in the contents of other major constituents such as carbonate (e.g. dilution effect)[3]. Accordingly it is important to convert barite abundance to barite accumulation rates (BAR). BAR are calculated as the product of the wt% barite and the bulk sediment mass accumulation rate (MAR). The MAR was calculated as the product of the dry bulk density obtained from ODP records and the sedimentation rate for each sample determined from $^{3}$He data and correlation of C isotopes. Dry bulk densities (DBD) for DSDP site 549 were not available so grape (gamma-ray attenuation porosity evaluator) density and a relationship between DBD grape density from site 1051 in the North Atlantic were used. DBD for site 1215 was from initial report. DBD for all other

sites were calculated in high resolution according to the relationship between grape density and dry bulk density which can get from the IODP MAD database (http://iodp.tamu.edu/janusweb/physprops/maddat.shtml).

*Screening for Diagenesis*

All samples in this study were screened for the presence of diagenetic barite by visual calcification of crystal size and morphology using the SEM[26, 29]as well as through chemical tests specifically S isotopes[31]. Many of the samples were also analyzed for Sr [32] and Ca[33] isotopes and for Sr/Ba ratios in barite[15] and all samples are consistent with a Paleocene-Eocene water column origin. An example of the barite particles can be seen in Figure S1.

*Age Models*

Establishing appropriate age models and sedimentation rates can be difficult and introduces errors if sedimentation rates vary on timescales shorter than the resolution they are calculated for (see Ref.[34]), carbonate dissolution and condensed sedimentary sequences may also introduce an age error during the PETM[35].

Due to the limitation of astronomical calibration and the lack of geologically well constrained radio isotopic dates for the P-E boundary, the absolute age for the PETM is still debated and the current understanding indicates that it is "floating" between ~55 and 55.9 Ma[35, 36, 37, 38]. In this study our aim focuses on paleoproductivity change during the

PETM events, thus we use a relative age for which 0 was set as the onset of CIE based the carbon isotope record of each of the sites, negative relative ages refer to the time before the onset of CIE while positive relative ages represent time after onset of CIE.

Age models were constructed based on $^{3}$He ages where they exist (Sites 690, 1266, and 1263 from Farley & Eltgroth[39], Murphy[40, 41]). Ages for Sites 525, 549, 738, 1051, 1209 and 1265 are based on bulk carbon isotope correlation to site 1266 and the $^{3}$He age model for that site. The age models for sites 1215, 1220, and 1211 are loosely based on the few carbon isotope values available, and thus have a large error. Sedimentation rates were derived based on these assigned ages (Figure S2). Data is shown in Figure S2 and provided in Table S1.

Similar trends in BAR are observed using other available age models although the magnitude of the BAR peaks depend on the age model used as BAR is a direct function of age model based sedimentation rates (Figure S3). In this figure, the age for Sites 549, 738 and 690 were based on the age model constructed by Nunes and Norris[42], while those at Site 1220 and 1221 are based on the carbon isotope derived age model from Nunes and Norris[43]. For samples from Walvis Ridge (sites 1263, 1265 and 1266) ages over the PETM were calculated from Röhl et al.[35] using an age model derived from orbital cycle chronology integrated records of site 690. Ages for site 1051 and 1215 were computed by "tying" published $\delta^{13}C_{carb}$[44, 45] to the $\delta^{13}C$ record at site 690

*Carbon isotopes*

The bulk carbon isotope were from Thomas and Shackleton[46] for site 525, Stott et al.[47] for site 549, Larrasoana et al.[48] Bains et al.[44] for site 690 and 1051, Murphy[11] for site 1209, Leon-Rodriguez and Dickens[45] for site 1215, Nunes and Norris[43] for site 1220 and 1221, Zachos et al.[38] for 1263 and 1265 while Murphy et al.[41] for site 1266.

*Export productivity reconstruction and global extrapolation*

Using the 30kyr smoothed BAR record we used the peak BAR (average of both peaks) during the PETM and the time represented by the peak export productivity (30-50 kyr) to calculate export productivity and C flux at each site using the relation between BAR and export productivity of Eagle et al[13]. The pre-PETM export productivity values were calculated from pre-PETM averaged available BAR data (Table S1). The Paleocene-Eocene oceans were divided into six ocean zones, in the light of modern[49, 50] and PETM water mass and ocean basin charachteristics[51]. Annual organic C flux was calculated by multiplying export production of representative sites for each ocean basin with the size of the specific basin. A pixel-selected method was used to acquire the proportion of each ocean zone, and the size was calculated by multiplying the global ocean size (70% of the earth surface) by the specific basin fraction. Modern ocean organic carbon flux was derived from the annual export productivity calculated by multiplying the primary productivity[50] by the f ratio[49], the six ocean zones consisted of 57 ocean provinces defined in the reference[50] (Table 1).

Table S1: Site Location and Paleo Productivity

| Site | Modern-Location | | Paleo-Geographic | | | Paleo-Productivity (g C $m^{-2}$ $yr^{-1}$) | |
|---|---|---|---|---|---|---|---|
| | Lat. | Long. | Depth (m) | Lat. | Long. | PETM | Post &Pre PETM |
| 1263 | -28.5 | 2.8 | 1400[a] | -35 | -10[h] | 38 | 15 |
| 1265 | -28.8 | 2.6 | ~2000[a] | | | 26 | |
| 1266 | -28.6 | 2.4 | 3000[a] | | | 21 | |
| 525 | -29 | 3 | 1300[b] | -36 | -9.5[h] | - | - |
| 1051 | 30.1 | -76.4 | 2000[c] | 28.6 | -65.3[c] | 31 | 14 |
| 549 | 49.1 | -13.1 | 3900[c] | 45 | -31.5[c] | 48 | 18 |
| 1215 | 26 | -143.7 | ~3000[d] | 11 | -112[i] | 148 | 20 |
| 1221 | 12 | -142.7 | ~3000[d] | 3.1 | -116.5[h] | 70 | |
| 1220 | 10.2 | -158.8 | ~2900[d] | 1.3 | -115.5[h] | 120 | |
| 1209 | 32.7 | 82.5 | ~550[e] | 23.5 | -171.1[h] | 14.5 | 13 |
| 738 | -62.7 | 1.8 | 1000[f] | -63.9 | 77.6[h] | - | - |
| 690 | -65.1 | -8.2 | 1900[g] | -65.6 | -7.2[h] | 33 | 17 |

The PETM export productivity in each site calculated based on the BAR (barite accumulation rates) and then did a 30 kyr smooth. Data from *a*:[52]; *b*:[53]; *c*:[54]; *d*:[43]; *e*:[55]; *f*:[56]; *g*:[57]; *h*:[51]; *i*:[58]

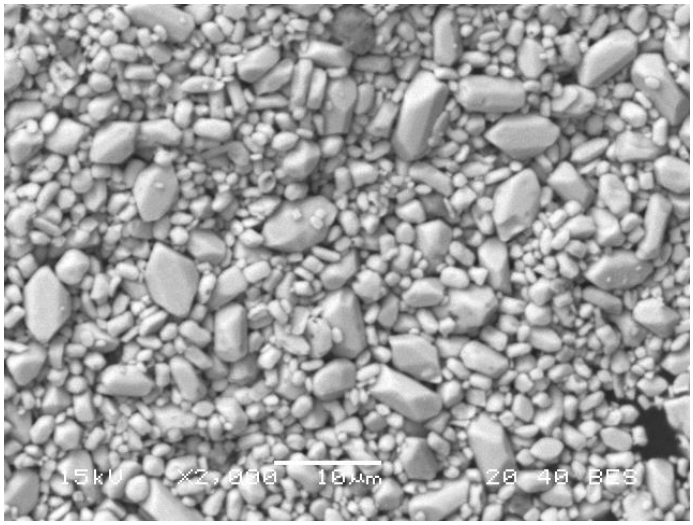


Figure S1: Scanning electron micrographs of marine barite separated from Site 1221C (154.06 mbsf; 1221C 11-3 66-70cm). Scale bars are 10 µm (1000x magnification). Image taken by Dr. E.M Griffith.

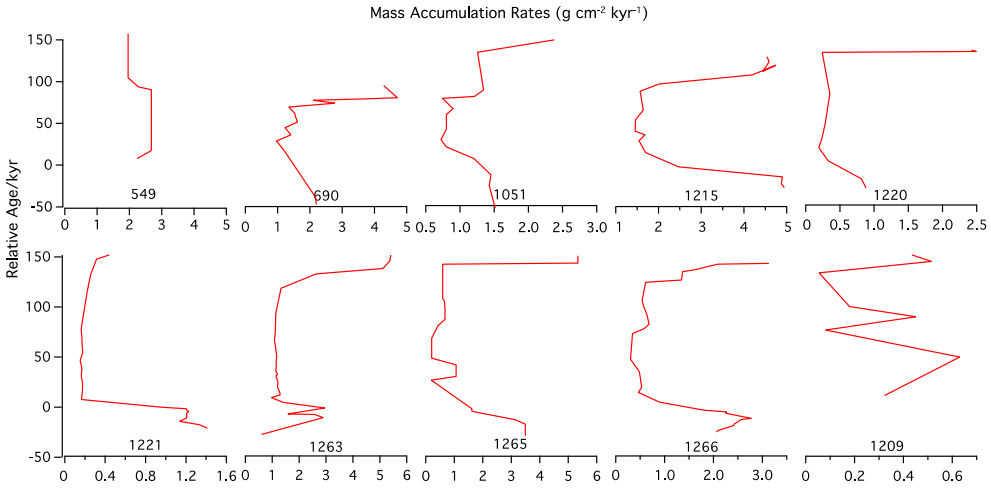


Figure S2: Mass accumulation rates at each site plotted against the relative age model where 0 is defined as the start of the start of the CIE.

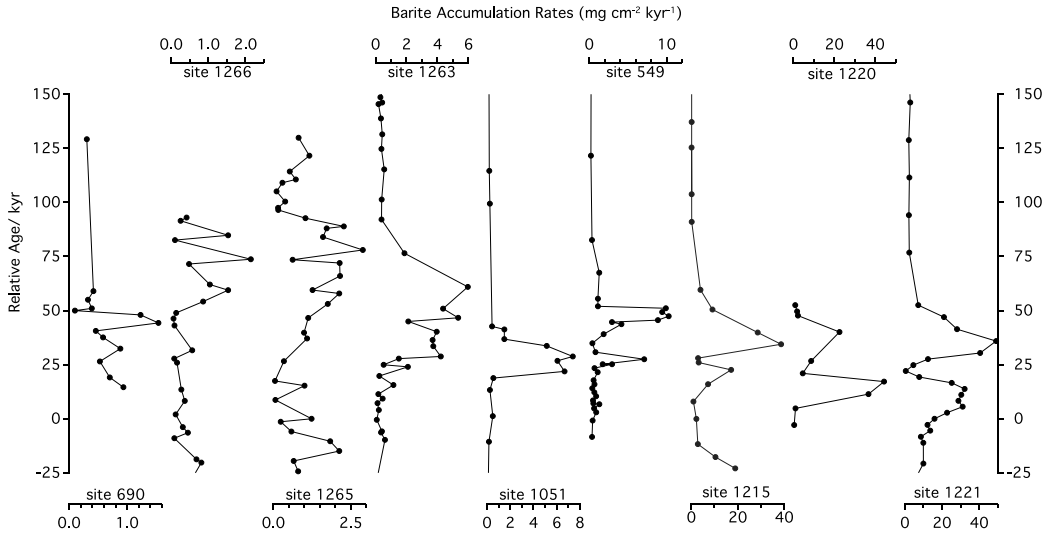


Figure S3: BAR at each site calculated based on non He based age models. Note that the peaks in BAR are still observed although the magnitude of the peaks and their exact position shift compare to the $^{3}$He based age model

**References:**


1. Bishop JKB. The barite-opal-organic carbon association in oceanic particulate matter. *Nature* 1988, **332**(6162)**:** 341-343.

2. Dymond J, Collier R. Particulate barium fluxes and their relationships to biological productivity. *Deep Sea Research Part II: Topical Studies in Oceanography* 1996, **43**(4-6)**:** 1283-1308.

3. Dymond J, Suess E, Lyle M. Barium in Deep-Sea Sediment: A Geochemical Proxy for Paleoproductivity. *Paleoceanography* 1992, **7**(2)**:** 163-181.

4. Dehairs F, Jacquet S, Savoye N, Van Mooy BAS, Buesseler KO, Bishop JKB, *et al.* Barium in twilight zone suspended matter as a potential proxy for particulate organic carbon remineralization: Results for the North Pacific. *Deep Sea Research Part II: Topical Studies in Oceanography* 2008, **55**(14-15)**:** 1673-1683.

5. Paytan A, Griffith EM. Marine barite: Recorder of variations in ocean export productivity. *Deep Sea Research Part II: Topical Studies in Oceanography* 2007, **54**(5-7)**:** 687-705.

6. Schmitz B. Barium, equatorial high productivity, and the northward wandering of the Indian continent. *Paleoceanography* 1987, **2**(1)**:** 63-77.

7. Rutsch HJ, Mangini A, Bonani G, Dittrich-Hannen B, Kubik PW, Suter M, *et al.* 10Be and Ba concentrations in West African sediments trace productivity in the past. *Earth and Planetary Science Letters* 1995, **133**(1-2)**:** 129-143.

8. Paytan A, Kastner M, Chavez FP. Glacial to Interglacial Fluctuations in Productivity in the Equatorial Pacific as Indicated by Marine Barite. *Science* 1996, **274**(5291)**:** 1355-1357.

9. Dean WE, Gardner JV, Piper DZ. Inorganic geochemical indicators of glacial-interglacial changes in productivity and anoxia on the California continental margin. *Geochimica et Cosmochimica Acta* 1997, **61**(21)**:** 4507-4518.

10. Nürnberg C, Bohrmann G, Schlüter M, Frank M. Barium accumulation in the Atlantic sector of the Southern Ocean: Results from 190,000‚Äêyear records. *Paleoceanography* 1997, **12**(4)**:** 594-603.

11. Bonn WJ, Gingele FX, Grobe H, Mackensen A, Fütterer DK. Palaeoproductivity at the Antarctic continental margin: opal and barium records for the last 400 ka. *Palaeogeography, Palaeoclimatology, Palaeoecology* 1998, **139**(3)**:** 195-211.

12. Bains S, Norris RD, Corfield RM, Faul KL. Termination of global warmth at the Palaeocene/Eocene boundary through productivity feedback. *Nature* 2000, **407**(6801)**:** 171-174.

13. Eagle M, Paytan A, Arrigo KR, van Dijken G, Murray RW. A comparison between excess barium and barite as indicators of carbon export. *Paleoceanography* 2003, **18**(1)**:** 21.21-21.13.

14. Gallego-Torres D, Martínez-Ruiz F, Paytan A, Jiménez-Espejo FJ, Ortega-Huertas M. Pliocene-Holocene evolution of depositional conditions in the eastern Mediterranean: Role of anoxia vs. productivity at time of sapropel deposition. *Palaeogeography, Palaeoclimatology, Palaeoecology* 2007, **246**(2-4)**:** 424-439.

15. Paytan A, Averyt K, Faul K, Gray E, Thomas E. Barite accumulation, ocean productivity, and Sr/Ba in barite across the Paleocene Eocene Thermal Maximum. *Geology* 2007, **35**(12)**:** 1139-1142.

16. Goldberg E, Arrhenius G. Chemistry of Pacific pelagic sediments. *Geochimica et Cosmochimica Acta* 1958, **13:** 153-198.

17. Arrhenius G. Sedimentation on the ocean floor. *Researches in geochemistry Wiley, New York* 1959, **1**.

18. Church TM. Marine barite. Ph. D thesis, University of California, San Diego, 1970.

19. Stecher HA, Kogut MB. Rapid barium removal in the Delaware estuary. *Geochimica et Cosmochimica Acta* 1999, **63**(7)**:** 1003-1012.

20. Ganeshram RS, François R, Commeau J, Brown-Leger SL. An experimental investigation of barite formation in seawater. *Geochimica et Cosmochimica Acta* 2003, **67**(14)**:** 2599-2605.

21. Dehairs F, Baeyens W, Goeyens L. Accumulation of Suspended Barite at Mesopelagic Depths and Export Production in the Southern Ocean. *Science* 1992, **258**(5086)**:** 1332-1335.

22. Dehairs F, Chesselet R, Jedwab J. Discrete suspended particles of barite and the barium cycle in the open ocean. *Earth and Planetary Science Letters* 1980, **49**(2)**:** 528-550.

23. Paytan A, Moore WS, Kastner M. Sedimentation rate as determined by 226Ra activity in marine barite. *Geochimica et Cosmochimica Acta* 1996, **60**(22)**:** 4313-4319.

24. McManus J, Berelson WM, Klinkhammer GP, Johnson KS, Coale KH, Anderson RF, *et al.* Geochemistry of barium in marine sediments: implications for its use as a paleoproxy. *Geochimica et Cosmochimica Acta* 1998, **62**(21-22)**:** 3453-3473.

25. McManus J, Berelson WM, Klinkhammer GP, Kilgore TE, Hammond DE. Remobilization of barium in continental margin sediments. *Geochimica et Cosmochimica Acta* 1994, **58**(22)**:** 4899-4907.

26. Paytan A, Kastner M, Campbell D, Thiemens MH. Seawater Sulfur Isotope Fluctuations in the Cretaceous *Science* 2004, **304:** 1663-1665.

27. Dickens GR. Carbon addition and removal during the Late Palaeocene Thermal Maximum: basic theory with a preliminary treatment of the isotope record at ODP Site 1051, Blake Nose. *Geological Society, London, Special Publications* 2001, **183**(1)**:** 293-305.

28. Dickens GR, Fewless T, Thomas E, Bralower TJ. Excess barite accumulation during the Paleocene-Eocene Thermal Maximum: Massive input of dissolved barium from seafloor gas hydrate reservoirs. In: Schmitz i, Thomas E, Gingerich PD, Wing SL (eds). *Causes and Consequences of Globally Warm Climates in the Early Paleogene*. Geological Society of America: Boulder, 2003.

29. Paytan A, Mearon S, Cobb K, Kastner M. Origin of marine barite deposits: Sr and S isotope characterization. *Geology* 2002, **30**(8)**:** 747-750.

30. Breit GN, Simmons EC, Goldhaber MB. Dissolution of barite for the analysis of strontium isotopes and other chemical and isotopic variations using aqueous

sodium carbonate. *Chemical Geology: Isotope Geoscience section* 1985, **52**(3-4)**:** 333-336.

31. Paytan A, Kastner M, Campbell D, Thiemens MH. Sulfur isotope composition of Cenozoic seawater sulfate. *Science* 1998, **282:** 1459-1462.

32. Paytan A, Kastner M, Martin EE, Macdougall JD, Herbert T. Marine barite as a monitor of seawater strontium isotope composition. *Nature* 1993, **366**(6454)**:** 445-449.

33. Griffith EM. Seawater calcium isotopes and the Cenozoic carbonate depositional history of the oceans. PhD thesis, Stanford University, 2008.

34. Anderson RF, Winckler G. Problems with paleoproductivity proxies. *Paleoceanography* 2005, **20**(3)**:** PA3012.

35. Röhl U, Westerhold T, Bralower TJ, Zachos JC. On the duration of the Paleocene-Eocene thermal maximum (PETM). *Geochem Geophys Geosyst* 2007, **8**(12)**:** Q12002.

36. Charles AJ, Condon DJ, Harding IC, Pälike H, Marshall JEA, Cui Y, *et al.* Constraints on the numerical age of the Paleocene-Eocene boundary. *Geochem Geophys Geosyst* 2011, **12:** Q0AA17.

37. Cui Y, Kump LR, Ridgwell AJ, Charles AJ, Junium CK, Diefendorf AF, *et al.* Slow release of fossil carbon during the Palaeocene-Eocene Thermal Maximum. *Nature Geosci* 2011, **4**(7)**:** 481-485.

38. Zachos JC, Röhl U, Schellenberg SA, Sluijs A, Hodell DA, Kelly DC, *et al.* Rapid Acidification of the Ocean During the Paleocene-Eocene Thermal Maximum. *Science* 2005, **308**(5728)**:** 1611-1615.

39. Farley K, Eltgroth S. An alternative age model for the Paleocene-Eocene thermal maximum using extraterrestrial 3He. *Earth and Planetary Science Letters* 2003, **208**(3)**:** 135-148.

40. Murphy BH. Insights Into the Pace and Paleoceanography of Early Eocene Events of Global Warming. Ph.D. thesis, University of California, Santa Cruz, Santa Cruz, 2011.

41. Murphy BH, Farley KA, Zachos JC. An extraterrestrial $^{3}$He-based timescale for the Paleocene-Eocene thermal maximum (PETM) from Walvis Ridge, IODP Site 1266. *Geochimica et Cosmochimica Acta* 2010, **74**(17)**:** 5098-5108.

42. Nunes F, Norris RD. Abrupt reversal in ocean overturning during the Palaeocene/Eocene warm period. *Nature* 2006, **439**(7072)**:** 60-63.

43. Nunes F, Norris RD. Data report: High-resolution stable isotope records across the Paleocene/Eocene boundary, ODP Sites 1220 and 1221. In: Wilson PA, Lyle M, Firth JV (eds). *Proc. ODP, Sci. Results*, vol. 199. Ocean Drilling Program: College Station, TX, 2005, pp 1-12.

44. Bains S, Corfield RM, Norris RD. Mechanisms of Climate Warming at the End of the Paleocene. *Science* 1999, **285**(5428)**:** 724-727.

45. Leon-Rodriguez L, Dickens GR. Constraints on ocean acidification associated with rapid and massive carbon injections: The early Paleogene record at ocean drilling program site 1215, equatorial Pacific Ocean. *Palaeogeography, Palaeoclimatology, Palaeoecology* 2010, **298**(3-4)**:** 409-420.

46. Thomas E, Shackleton NJ. The Paleocene-Eocene benthic foraminiferal extinction and stable isotope anomalies. *Geological Society, London, Special Publications* 1996, **101**(1)**:** 401-441.

47. Stott LD, Sinha A, Thiry M, Aubry M-P, Berggren WA. Global d13C changes across the Paleocene-Eocene boundary: criteria for terrestrial-marine correlations. *Geological Society, London, Special Publications* 1996, **101**(1)**:** 381-399.

48. Larrasoaña JC, Roberts AP, Chang L, Schellenberg SA, Fitz Gerald JD, Norris RD, *et al.* Magnetotactic bacterial response to Antarctic dust supply during the Palaeocene-Eocene thermal maximum. *Earth and Planetary Science Letters* 2012, **333:** 122-133.

49. Laws EA, Falkowski PG, Smith WO, Jr., Ducklow H, McCarthy JJ. Temperature Effects on Export Production in the Open Ocean. *Global Biogeochem Cycles* 2000, **14**(4)**:** 1231-1246.

50. Longhurst A, Sathyendranath S, Platt T, Caverhill C. An estimate of global primary production in the ocean from satellite radiometer data. *J Plankton Res* 1995, **17**(6)**:** 1245-1271.

51. Winguth AME, Thomas E, Winguth C. Global decline in ocean ventilation, oxygenation, and productivity during the Paleocene-Eocene Thermal Maximum: Implications for the benthic extinction. *Geology* 2012, **40**(3): 63–266.

52. Zachos JC, Kroon D, Blum P. *Proc. ODP, Init. Repts. 208*: College Station, TX (Ocean Drilling Program). 2004.

53. Li L, Keller G. Abrupt deep-sea warming at the end of the Cretaceous. *Geology* 1998, **26**(11)**:** 995-998.

54. Thomas DJ, Bralower TJ, Jones CE. Neodymium isotopic reconstruction of late Paleocene-early Eocene thermohaline circulation. *Earth and Planetary Science Letters* 2003, **209**(3-4)**:** 309-322.

55. Bralower TJ, Silva IP, Malone MJ. New evidence for abrupt climate change in the Cretaceous and Paleogene: An Ocean Drilling Program expedition to Shatsky Rise, northwest Pacific. *GSA Today* 2002, **12**(11)**:** 4-10.

56. Wei W, Pospichal J. Danian calcareous nannofossil succession at Site 738 in the southern Indian Ocean. Proceedings of the Ocean Drilling Program, Scientific Results; 1991; 1991. p. 495-512.

57. Thomas E. Late Cretaceous through Neogene deep-sea benthic foraminifers (Maud Rise, Weddell Sea, Antarctica). Proceedings of the Ocean Drilling Program, Scientific Results; 1990; 1990. p. 571-594.

58. Ziegler CL, Murray RW, Hovan SA, Rea DK. Resolving eolian, volcanogenic, and authigenic components in pelagic sediment from the Pacific Ocean. *Earth and Planetary Science Letters* 2007, **254**(3-4)**:** 416-432.